A Study of Self-excited Oscillations of the Tropical Ocean–Atmosphere System. Part II: Nonlinear Cases*

MATTHIAS MÜNNICH, MARK A. CANE AND STEPHEN E. ZEBIAK

Lamont-Doherty Geological Observatory of Columbia University, Palisades, New York

(Manuscript received 10 July 1990, in final form 3 December 1990)

ABSTRACT

We study the behavior of an iterative map as a model for El Niño and the Southern Oscillation (ENSO). This map is derived from a model that combines linear equatorial beta-plane ocean dynamics with a version of the Bjerknes hypothesis for ENSO. It differs from the linear model of Cane et al. only in that the coupling from ocean to atmosphere is idealized as a *nonlinear* relation $\tau(h_e)$ between a wind stress τ of fixed spatial form and h_e, the thermocline displacement at the eastern end of the equator. The model sustains finite amplitude periodic and aperiodic oscillations. A period doubling bifurcation leads from a period of less than 2 years to the 3–4 year one observed in nature. Other principal results are: the resulting period depends on the curvature of the function away from the unstable equilibrium at $h_e = 0$, and not solely on its linear instability; at least two Rossby modes must be included in the model for aperiodic oscillations to appear; no stochastic term is needed for this aperiodicity, but it appears more readily if the model background state includes an annual cycle.

1. Introduction

In recent years the explanations for El Niño–Southern Oscillation (ENSO) have focused on the hypothesis of Bjerknes (1969) regarding ENSO as a positive feedback interaction between the tropical Pacific and the atmosphere above it. Various numerical models incorporating Bjerknes' idea were developed that showed a number of similarities with ENSO (especially Zebiak and Cane 1987; Schopf and Suarez 1988; and Battisti 1988). In order to explain the behavior of these numerical models highly simplified models were created in attempts to capture the essence of the numerical model oscillations. The models of Battisti and Hirst (1989) and Suarez and Schopf (1988) fall in this category.

In Cane et al. (1990, henceforth CMZ) we put forward such a simple model and analyzed its linear version. It has h_e, the thermocline height anomaly at the eastern end of the equator, as its single dependent variable. If $h_e > 0$ the thermocline is deeper than usual and the sea surface temperature warmer, as in an El Niño event. The warming in the east reduces the east–west temperature contrast along the equator, which causes the easterly wind to weaken, in accord with Bjerknes' ideas. The CMZ model retains only the essence of the complex ocean–atmosphere physics implicit in this description: a linear shallow water equatorial ocean is driven by a wind stress of fixed form whose amplitude depends only on h_e.

The CMZ model gives growing oscillations or pure growth depending mainly on the coupling strength between ocean and atmosphere. In contrast to the results of the more complete nonlinear numerical model of Zebiak and Cane (1987, henceforth ZC), we found that a small change in parameter values changes the period from 2 years to infinity. Such behavior is characteristic of the other simple linear models as well; viz. Fig. 2 of Battisti and Hirst (1989). Since these models are such far reaching simplifications of reality—or even of the numerical models—"realistic" values of parameters cannot be determined with precision. We therefore feel that the linear models such as CMZ do not provide a sufficient explanation for the ENSO time scale. So either CMZ does not capture the basic mechanism for ENSO or nonlinear effects are crucial in determining the period range of ENSO. The latter may well be the case, as we shall see below.

The remainder of this paper is organized as follows. Section 2 reviews the iterative map obtained in CMZ and shows how to include friction in the model. In Section 3 we present results from calculations with this model. Section 4 is a summary and discussion. The Appendix gives a derivation of our model from the shallow water equations.

2. The model

In this section the iterated map we study will be derived from the model equation in the companion paper CMZ. We review briefly this inviscid model and add Raleigh friction. The Appendix gives a more complete derivation.

* Lamont-Doherty Geological Observatory Contribution Number 4746.

Corresponding author address: Dr. Mark Cane, Lamont-Doherty Geological Observatory, Columbia University, Palisades, NY 10964.

The ocean dynamics of the CMZ model are governed by linear shallow water equation on an equatorial beta-plane. The ocean is meridionally infinite and zonally bounded by meridional walls. The forcing wind stress τ is chosen to be only zonal with the fixed spatial structure

$$\tau = A(t)e^{-(\mu/2)y^2}f(x) \qquad (1)$$

where x denotes zonal, y meridional distance. The amplitude A at each time is taken to be solely dependent on the thermocline height at the eastern boundary, h_e, except that in some cases it will also depend on the time of year. As discussed in CMZ this is a simple version of Bjerknes' (1969) hypothesis for ENSO.

Cane et al. (1990) was devoted to the case of linear forcing $A(h_e) = \kappa h_e$. It was shown that the resulting low-frequency ocean response is nearly independent of the zonal forcing structure $f(x)$ over the ocean as long as the mean forcing strength over the ocean and the zonal center of the stress are kept the same. The appendix to Schopf and Suarez (1990) gives an explanation for this independence. This allowed us to pick $f(x)$ for convenience. We chose an infinitely narrow forcing at $x = x_0$ $(0 < x_0 < 1)$; i.e., $f(x) = \delta(x - x_0)$ and derived for that the following equation for the Fourier transform of h_e [CMZ eq. (45)]:

$$\hat{h}_e(\omega) = \sum_{j=1}^{\infty} a_j^+ z^{4j}\hat{h}_e(\omega) + \frac{1}{(1+\mu)^{1/2}}(z^{1-x_0} + z\sum_{j=1}^{\infty} z^{(4j-1)x_0}[a_j^- \nu^j - a_{j-1}^- \nu^{j-1}])\hat{A}(\omega) \qquad (2)$$

with

$$\nu = \frac{1-\mu}{1+\mu}, \quad z = e^{-i\omega},$$

and the $a_j^{\pm}$ defined by

$$(1-x)^{\pm 1/2} = 1 \mp \sum_{j=1}^{\infty} a_j^{\pm} x^j.$$

We transform this back into the time domain, and include a Rayleigh friction r as shown in the Appendix. The result is

$$h_e(t) = \sum_{j=1}^{\infty} a_j^+ e^{-4jr}h_e(t-4j) + \frac{1}{(1+\mu)^{1/2}}e^{-(1-x_0)r}A[t-(1-x_0)] + \frac{1}{(1+\mu)^{1/2}}\sum_{j=1}^{\infty} e^{-[1+(4j-1)x_0]r}[a_j^-\nu^j - a_{j-1}^-\nu^{j-1}] \times A\{t-[1+(4j-1)x_0]\}. \qquad (3)$$

As one can see from the Appendix the sum in (3) extends over the odd Rossby waves. We neglect higher Rossby waves $j > N$ and assume x_0 to be rational: $x_0 = k/l$ with integer k, l. If we rescale time by $1/l$ and evaluate a^+, a^- we get

$$(1+\mu)^{1/2}h_e(t) = e^{-(1-k/l)r}A(t-[l-k]) - \sum_{j=1}^{N} b_j a_j(\mu)e^{-(1+[4j-1]k/l)r}A\{t-[2+(4j-1)k]\} + (1+\mu)^{1/2}\sum_{j=1}^{N} b_j e^{-4jr}h_e(t-4jl) \qquad (4)$$

with $b_j = a_j^+$; i.e.

$$b_1 = \frac{1}{2}, \quad b_j = \frac{1\cdot 3\cdot 5\cdot \cdots \cdot(2j-3)}{2\cdot 4\cdot 6\cdot \cdots \cdot 2j};$$

and

$$a_j(\mu) = \left(\frac{1-\mu}{1+\mu}\right)^{j-1}\frac{[(4j-1)\mu+1]}{1+\mu};$$

$$A(t) = A(h_e(t), t).$$

This is a recursive equation for $h_e(t)$. If $A(h_e(t), t)$ is specified, h_e is determined for all times by $h_e(t), \ldots, h_e(t-4Nl+1)$. It can be written in the form

$$\mathbf{h}(n+1) = \mathbf{F}(\mathbf{h}(n))$$

$$\mathbf{h}(n) = \begin{pmatrix} h_e(t=n) \\ h_e(t=n-1) \\ \vdots \\ h_e(t=n-4Nl+1) \end{pmatrix} \qquad (5)$$

with a fixed map $\mathbf{F}$: $R^{4Nl} \to R^{4Nl}$. Iterating (5) we get a time sequence for h_e at discrete points in time. The behavior of such iterative maps is studied in dynamical systems theory (see Collet and Eckmann 1980), but most of the results deal only with one-dimensional maps. Here we study (5) experimentally, by computing the resulting time sequences for different $A(h_e)$.

3. Results from computer experiments

If the zonal structure of the real wind is $f(x)$, then the best choice for x_0 is $x_0 = \int_0^1 x f(x)dx$. For our numerical study we fix the location of the forcing to be in the center of the basin ($x_0 = \frac{1}{2}$). This is a realistic choice, and because of the small value for l, it has the advantage of leading to the simplest version of (4):

$$(1+\mu)^{1/2}h_e(t) = e^{-r/2}A(t-1) - \sum_{n=1}^{N} b_n a_n(\mu)e^{-(4n+1)r/2}A(t-4n-1) + (1+\mu)^{1/2}\sum_{n=1}^{N} b_n e^{-4nr/2}h_e(t-4n). \qquad (6)$$

The damping time is set to 30 months; for the Pacific time scale (Kelvin wave crossing time) of 2.3 month,

$r = 0.076$. The parameter μ controlling the meridional width is set to 0.1, which corresponds to an e-folding scale of $\sim 15°$.

a. Forcing with cubic nonlinearity

The case of linear forcing $A(h_e) = \kappa h_e$ was thoroughly analysed in CMZ. We add to this a cubic nonlinearity:

$$A(h'_e) = \kappa'(h'_e - \alpha h'^3_e) \tag{7}$$

We can eliminate the second parameter by rescaling h'_e and κ': define $h_e = \alpha^{1/2} h'_e$; $\kappa = \alpha^{-1/2}\kappa'$. In these new variables (7) becomes

$$A(h_e) = \kappa(h_e - h_e^3). \tag{8}$$

Figures 1a–f show the resulting time sequences for different κ. The series in (6) are truncated at $N = 10$ and the initial condition here, as in all the following runs, is $h(t = 0) = 10^{-4}$; $h(t < 0) = 0$.

As the coupling parameter κ is increased the resulting time sequences goes through the following regimes:

(i) For κ small ($\kappa < 1.2$) the feedback is too weak to sustain oscillations. The system shows dying oscillations due to Raleigh friction.

(ii) For $1.2 < \kappa < 1.88$ we obtain finite amplitude periodic oscillations. The periods increase from 1.5 years for $\kappa = 1.2$ to 2.1 years for $\kappa = 1.88$. In the linear case, (CMZ Fig. 2) for this relatively small parameter interval the period ranged from 1.6 years for $\kappa = 1.2$ to infinity for $\kappa > 1.7$. Comparing the linear and nonlinear results, we conclude that the nonlinearity shortens the periods for stronger coupling. Hence there is less sensitivity to the coupling strength in the nonlinear case.

(iii) If $\kappa > 1.89$ the nonlinearity alters the behavior of the model considerably. Without the nonlinearity we would be in a regime of pure growth. Now we observe a bifurcation. The period doubles from 2.1 years for $\kappa = 1.88$ to 4.2 years for $\kappa = 1.89$. The shape of the oscillation changes as well, now showing a double maximum on each side of the cycle. The period becomes nearly independent of κ for $1.89 < \kappa < 2.14$ (not shown). It decreases to 3.75 years as κ increases from 1.89 to 2, and then increases to 3.8 years at $\kappa = 2.14$.

(iv) At $\kappa = 2.15$ the model has another bifurcation. The period jumps to 5.5 years and the time sequence now shows many spikes on each side of the cycle. These

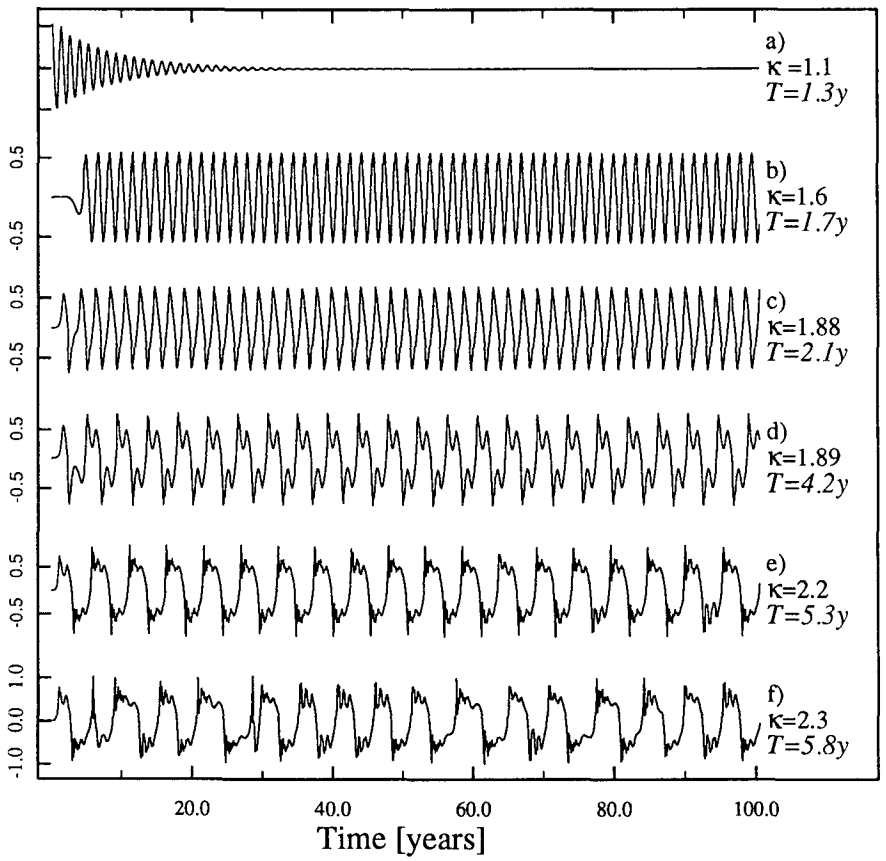

FIG. 1. Time sequences of $h(t)$ for cubic forcing $\tau = \kappa(h - h^3)$ and different κ. T, the average period in years, is determined from the output.

peaks change from cycle to cycle making the sequence not perfectly periodic, although the fundamental period remains fixed.

(v) For $\kappa \geq 2.29$ this is no longer true: the aperiodic oscillations dominate.

(vi) Finally, at $\kappa = 2.31$ the system becomes unstable and the time sequence goes to infinity.

To summarize: for small values of the coupling parameter κ the system has a fixed point ($h = 0$). As κ is increased there is a Hopf bifurcation to a periodic orbit. At still larger values of κ there is a second bifurcation to a period doubling. As κ is increased further a third bifurcation brings aperiodic behavior. Thus the dynamical system described by (6) and (8) appears to be following what Eckmann (1981) has termed the Ruelle–Takens–Newhouse road to chaos.

b. *A more realistic forcing function*

A cubic nonlinearity is a quite natural choice (viz. Schopf and Suarez 1989). It is the lowest order nonlinear antisymmetric forcing and so will be a good approximation to the real forcing as long as the nonlinearity is weak. But for $\kappa \geq 1.6$, a range suggested by the ZC model, this is not the case. For $\kappa > 1.7$ the amplitude of h_e becomes larger than $3^{-1/2}$, where the cubic forcing reaches its maximum value. So in these cases the forcing actually decreases before the anomaly reaches its maximum, an unphysical behavior. For $\kappa > 2.2$ the amplitude of h_e becomes so big that the wind stress anomaly actually reverses its sign. We must rule out the possibility that it is this unrealistic property of the forcing that is responsible for the bifurcation and aperiodicity.

To this end, we change the forcing function in the remainder of our numerical study to the following:

$$A(h) = \begin{cases} b_+ + \dfrac{b_+}{a_+}\left\{\tanh\left[\dfrac{\kappa a_+}{b_+}(h - h_+)\right] - 1\right\}, & h_+ < h \\ \kappa h, \quad h_- \leq h \leq h_+ & \\ -b_- - \dfrac{b_-}{a_-}\left\{\tanh\left[\dfrac{\kappa a_-}{b_-}(h - h_-)\right] - 1\right\}, & h < h_-. \end{cases} \tag{9}$$

We must have $a_\pm > 1$ and

$$h_+ = \frac{b_+}{\kappa a_+}(a_+ - 1); \quad h_- = \frac{-b_-}{\kappa a_-}(a_- - 1) \tag{10}$$

in order to ensure that $A(h)$ is continuous. The function (9), a linear piece inserted smoothly between two tanh segments, is fashioned after the shape of the tropical thermocline (viz. Fig. 2 on its side; also see ZC). It has the following desirable properties. It is three times differentiable and strictly monotonically increasing: as $h \to \pm\infty$, $A \to \pm b_\pm$. Without loss of generality we may take $b_+ = 1$. If the function is symmetric ($b_- = 1$), then it is determined by κ and $a_\pm$. In the linear stability analysis of CMZ, κ (the slope at $h = 0$), was the paramount parameter. In the present nonlinear case we add $a_\pm$, which control the curvature of $A(h)$, i.e., how rapidly A approaches the asymptotic values $b_\pm$. The larger $a_\pm$ are, the faster these limits are reached, with its limit function as $a_+, a_- \to \infty$ being the piecewise linear form

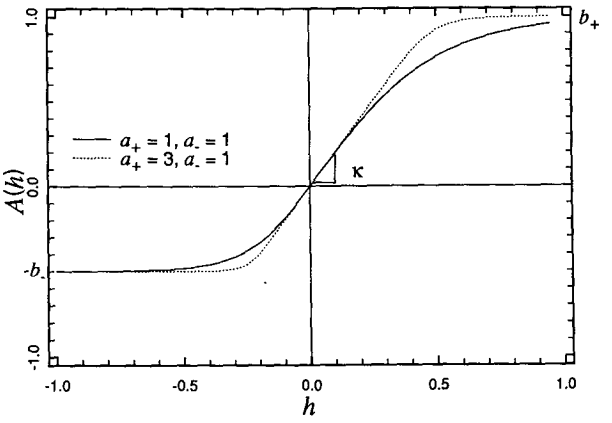

FIG. 2. Forcing function $A(h)$ given by Eq. (9).

$$A(h) = \begin{cases} b_+, & h > \dfrac{b_+}{\kappa} \\ \kappa h, & \dfrac{-b_-}{\kappa} \leq h \leq \dfrac{b_+}{\kappa} \\ -b_-, & h < -\dfrac{b_-}{\kappa}. \end{cases} \tag{11}$$

We first consider the case of symmetric forcing: $a_+ = a_-$, $b_+ = -b_- = 1$. Choosing $a_\pm = 1$ we increase κ, a measure of the instability of the system at $h = 0$. Figure 3a shows the resulting time sequences for different κ. The model undergoes the same bifurcations as in the case of cubic forcing: After κ is big enough ($\kappa > 1.2$) to sustain a finite amplitude oscillation it oscillates with periods between 1.3 years (for $\kappa = 1.2$) to 2.2 years for $\kappa = 2.25$, where the period doubles to 4.5 years. Increasing κ further reduces the period to 4.0 years. At $\kappa = 2.66$ the system undergoes another bifurcation, the period increasing to 6.7 years, roughly triple the value for small κ. Further increases in κ up to $\kappa = 2.83$ reduce the period slightly, but leave the qualitative behavior unchanged. At $\kappa = 2.84$ the system locks into a steady warm state. No aperiodic behavior appears in this sequence.

Figure 3b shows a similar set of runs, but with increased curvature: $a_\pm = 2$. There is similar sequence of bifurcations, but the transitions occur at lower values of κ. Also, aperiodic behavior now appears for $\kappa \geq 2.33$.

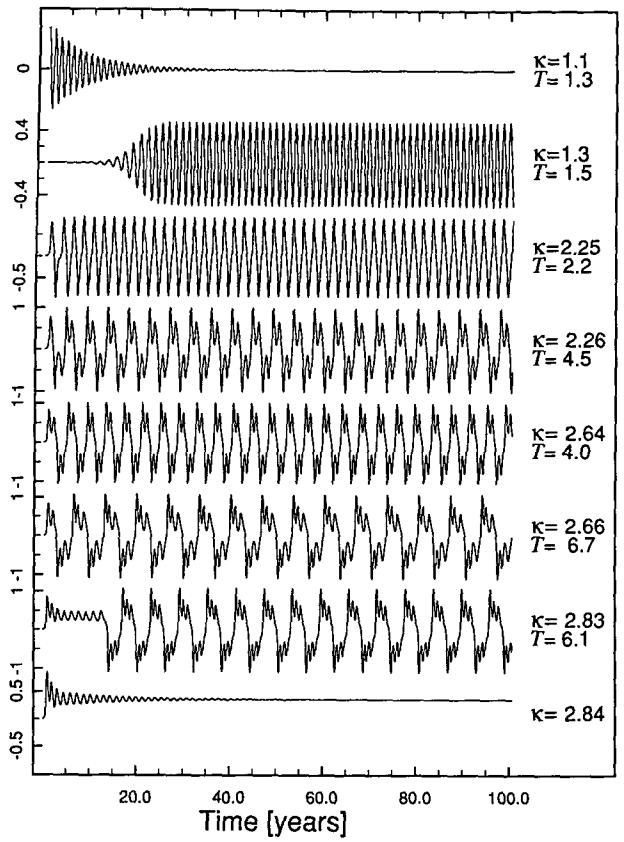

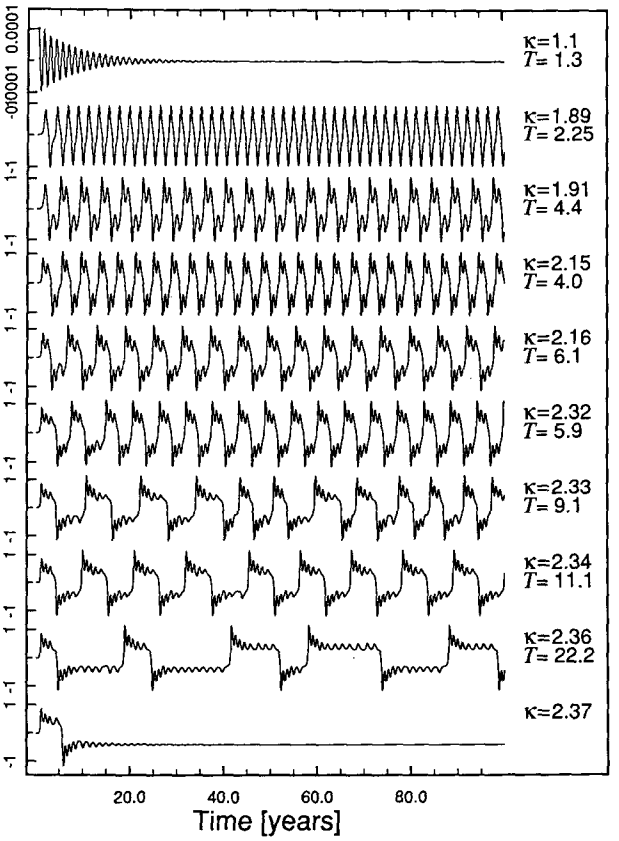

FIG. 3. $h(t)$ for the symmetric forcing function $|b_\pm| = 1$ without an annual cycle and various κ; cf. Fig. 2 and Eq. (9). Ten Rossby waves included. T, the average period in years, is determined from the output. (a) $a_\pm = 1$, (b) $a_\pm = 2$.

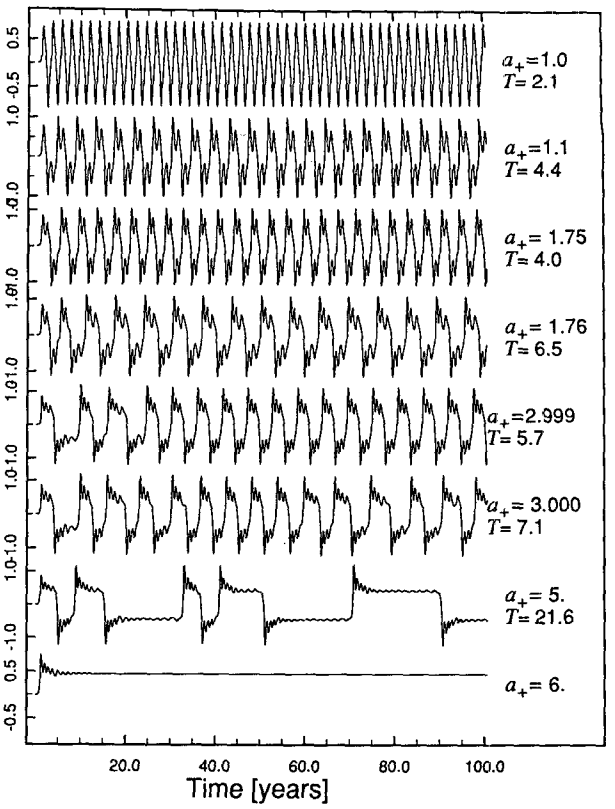

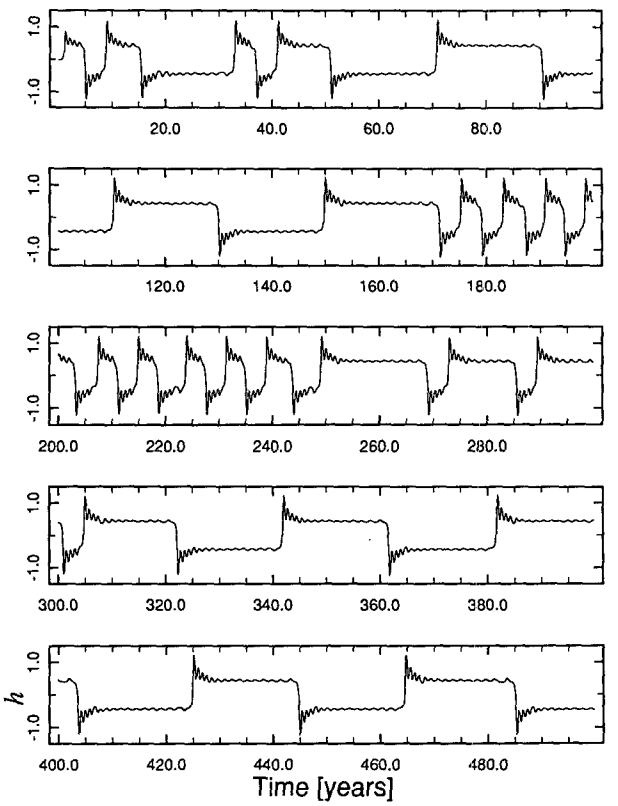

FIG. 4. (a) $h(t)$ for the symmetric forcing function ($a_+ = a_-$; $b_+ = -b_- = 1$), varying the curvature of the forcing ($a_\pm$). $N = 10$ and $\kappa = 2.2$. T gives the average period in years. (b) A 500-year sequence for the case $a_\pm = 5$.

We conclude that the bifurcations are not simply an artifact of the unphysical weakening allowed in the cubic case, but are typical for the system. In fact, we found them for many different forcing functions. Furthermore, the differences between $a_\pm = 1$ and $a_\pm = 2$ show that these bifurcations are not determined solely by the degree of instability at $h = 0$. Note that we increased the curvature of $A(h)$ in Fig. 1 and Fig. 3 by increasing κ. We now make another parameter study, where we increase $a_\pm$, keeping κ fixed. This will increase the curvature of $A(h)$ around $h_\pm$ but not its slope at $h = 0$. The resulting sequences for fixed $\kappa = 2.2$ are shown in Fig. 4a.

Again the system shows the same kind of parameter dependence: a period doubling at $a_\pm = 1.1$ and another bifurcation at $a_\pm = 1.76$. For $a_\pm > 3.0$ aperiodic time sequences appear. For $a_\pm \geq 6.0$ the time sequence goes towards a new equilibrium state. Clearly, the slope at $h = 0$ is not the only parameter influencing the period. The curvature—how fast the forcing levels off towards its maximum value—can determine how long the resulting period of the model will be and whether it will be periodic or not. In fact, for a piecewise linear function like (11) we observe aperiodic behavior for a very wide range of κ. It is not uncommon in dynamical systems for changes in a variety of parameters to yield the same range of qualitative behaviors.

The rather bizarre behavior at $a_\pm = 5$ is illustrated at greater length in Fig. 4b. Remarkably, the value of h_e can remain roughly constant for almost 15 years and then make a rapid transition to another state. Recall that h_e is the only variable in this model system, and that with the friction we use 15-year-old information has been reduced by a factor of e^{-6}. Therefore, it must be the very small irregularities of the quasi-constant period that jolt it into a new regime. We see no obvious feature predicting that the transition will occur, for example, at $T = 90$ rather than $T = 85$. Our model system is obviously quite sensitive to initial conditions.

c. *Necessary number of Rossby waves*

We want to see how many Rossby waves N must be included in our model (7) to obtain aperiodicity. Suarez and Schopf (1988) and Battisti and Hirst (1989) use only one delay time and so include only one effective Rossby wave. They observe neither bifurcations nor aperiodicities in their models. The existence of more than one Rossby wave may be crucial for these richer behaviors. Indeed, with $N = 1$ our model always has a rather short period of 1.2–1.8 years. No period doubling or quasi-periodic behaviors are observed.

The number of Rossby waves is closely related to the dimensionality of the system and so gives an upper bound for its dimension. From (6) we know that for every Rossby wave included we increase the dimension of the map **F** by 8—a large increase of dimensionality. Varying the parameters of $A(h)$ in (9) we find that we need at least four Rossby waves to observe the first bifurcation. For $N < 4$ the time sequence either oscillates quite rapidly—showing periods of 1.2–2 years—or it converges toward a new equilibrium. For $N = 4$ the model again shows the characteristic period doubling and aperiodic behavior, but it behaves this way only for a small interval of κ or $a_\pm$. This parameter range widens considerably if we increase the number of Rossby waves. Figure 5a shows an example of doubled and tripled periods, but no aperiodicity (the $N = 7$ behavior is transient). For the parameter setting of Fig. 5b aperiodicity appears at $N = 8$.

d. *Annual cycle*

The matter is different if we include an annual cycle in the forcing by making κ time dependent:

$$\kappa(t) = \kappa_0\left[1 + B\cos\left(\frac{2\pi}{1\text{ yr}}t\right)\right]. \qquad (12)$$

This form takes crude account of the mean annual cycle in such factors as SST and wind speed. [Zebiak and Cane (1987) and Battisti (1988) offer some discussion of how the ocean–atmosphere coupling varies over the course of the year.] We now find an aperiodic time sequence for only two Rossby waves (Fig. 6). Apparently this more interesting behavior occurs only for well selected parameter values. The chaotic islands in the parameter space are small. We cannot exclude the possibility that these islands exist for $N = 1$ but are so small that we did not see them.

e. *Asymmetric forcing function*

The forcing function in the real world is not symmetric around the mean state. A positive thermocline anomaly might move the intertropical convergence zone towards the equator and so reduce the easterlies over the central Pacific. The effect for a negative thermocline anomaly is much weaker, so the resulting wind anomaly is much weaker. We can implement this by choosing $b_- < b_+$; the resulting time sequences show eventlike oscillations. The system stays much longer on the negative side close to 0 and shows short strong positive anomalies (Fig. 7 top). This is more in keeping with the character of the observed ENSO cycle.

If we add an annual cycle in κ the periodic oscillation becomes aperiodic (Fig. 7 middle). But the annual cycle is not essential for the aperiodicity. Figure 7 (bottom) shows an aperiodic oscillation without an annual cycle in κ. Apparently, adding the more realistic feature of asymmetry encourages aperiodicity. Finally, we note that the combination of asymmetry and an annual cycle (Fig. 8) allows the iterated map (6) studied here to rival the more physically complete ENSO model of Zebiak and Cane (1987) in the apparent chaos it can generate.

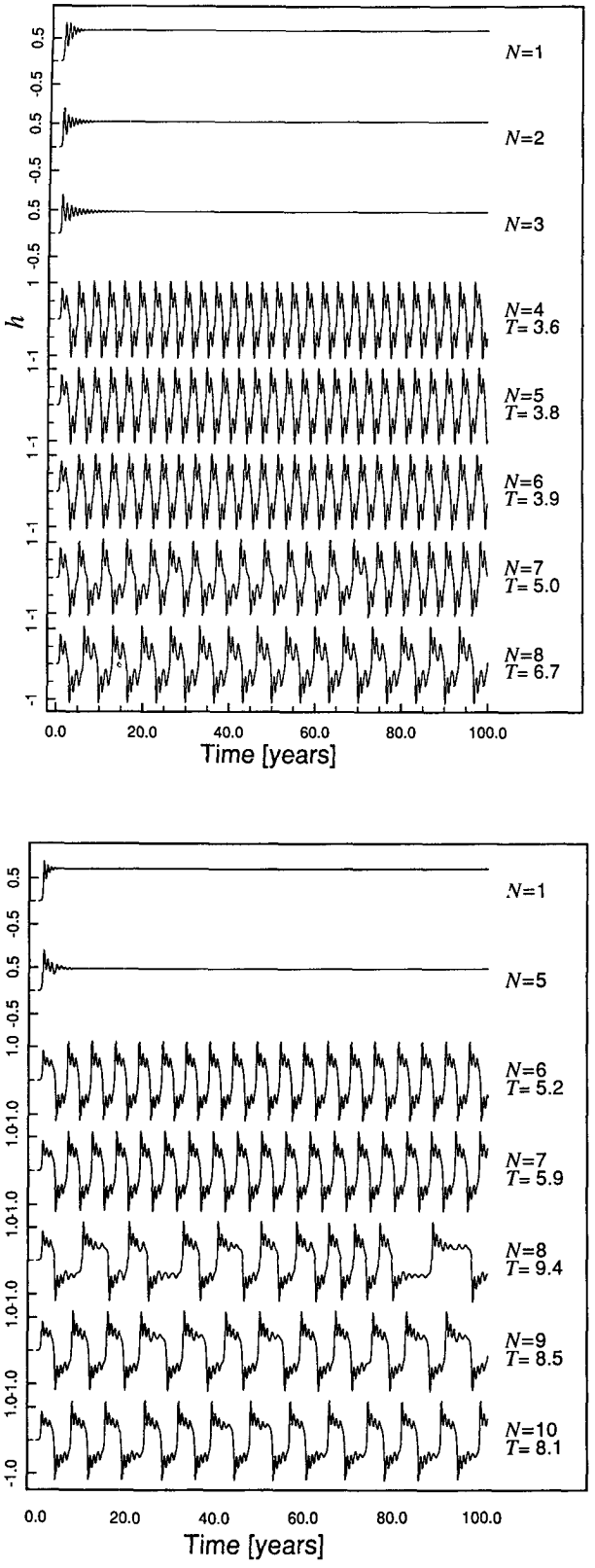

FIG. 5. $h(t)$ for the symmetric forcing function varying the number of Rossby waves. (a) $\kappa = 2.7$, $a_\pm = b_\pm = 1$; (b) $\kappa = 2.2$, $a_\pm = 3.5$, $b_\pm = 1$.

4. Discussion

In this paper we propose an iterated map as a possible paradigm for the El Niño–Southern Oscillation. It is a distillation of the Bjerknes (1969) scenario for ENSO, as amended by Wyrtki (1975) to emphasize the role of remote wind forcing and the equatorial waveguide. [Cane (1986) provides historical background.] The map is derived as the solution for wind-forced motions described by the shallow water equations on an equatorial beta-plane. The wind forcing is purely zonal, is centered longitudinally in the model ocean basin, and has fixed spatial form: infinitely thin in the longitudinal direction and Gaussian in latitude. The wind amplitude A depends solely on the thermocline height in the east, h_e. In a previous paper, Cane et al. (1990) presented the model used here and thoroughly analyzed the case where A is linearly related to h_e.

Here we numerically investigate cases where the relation $A(h_e)$ is nonlinear. While there are many physical features making the coupling between the tropical ocean and atmosphere nonlinear (e.g., cf. Zebiak and Cane 1987), we will mention only the one we believe to be most important: the vertical temperature profile in the upper layers of the tropical ocean does not have a constant gradient. (It resembles Fig. 2 turned on its side. This of course is not accidental.) Consequently, a given change in thermocline displacement has a variable effect on the sea surface temperature and hence on the atmospheric circulation, depending on how close the thermocline—the region of maximum gradient—is to the surface.

The nonlinear model exhibits a rich behavior, notably including finite amplitude oscillations with periods between 1.3 and 6 years. If the coupling between atmosphere and ocean is very weak the solution is a fixed point ($h_e = 0$). As it increases a bifurcation point is passed and simple periodic oscillations with periods of approximately 2 years appear. A further increase leads to a second bifurcation and a period doubling to 3–4 years, the mean period observed in nature. The shape of the oscillations changes from nearly sinusoidal to one with multiple extrema on either side of the cycle. That is, a quasi-biennial period is still evident. A further increase produces a third bifurcation, after which aperiodic behavior is observed. This sequence seemingly conforms to the Ruelle–Takens–Newhouse ("period 3 is chaos") scenario for the onset of chaos.

By varying the shape of the relation $A(h_e)$, the same qualitative sequence may be obtained even if the coupling strength dA/dh_e in the neighborhood of $h_e = 0$ is kept fixed. The parameter regimes showing aperiodic behavior widen, if we include an annual cycle in the forcing, and narrow, if we diminish the number of Rossby waves included. A minimum of two Rossby waves appear to be necessary to obtain aperiodicity; for only one Rossby wave the system either oscillates with a short period (less than 2 years), or converges toward a new equilibrium.

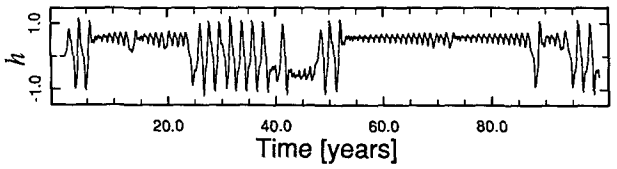

FIG. 6. $h(t)$ for the symmetric version of function (9) with an annual cycle and 2 Rossby waves. $N = 2$, $a_{\pm} = 7$, $b_{\pm} = 1$, $B = 0.25$, $\kappa = 1.9$.

The most striking result is the aperiodic oscillation of our model without stochastic forcing. Though not strictly necessary for aperiodicity to appear, incorporating an annual cycle or an asymmetry in the forcing makes it appear more readily. If this is true in the real world, then we may regard ENSO as a deterministic chaotic system.

The same idea has been expressed before, notably by Vallis (1986, 1988). However, there is little evidence that the simple models he studies characterize the way ENSO works in the real world. In contrast, as noted in the Introduction, there is a considerable body of work suggesting that the mechanisms incorporated into the model presented here are the ones crucial for ENSO. It is certain that they apply in *models* of ENSO that include complex ocean and atmosphere physics and show a fair degree of verisimilitude. Indeed, one of these models has been used to predict El Niño events (Cane et al. 1986; Barnett et al. 1988).

We do not claim that the iterated map presented here is a realistic model, but do suggest that it is a proper paradigm for ENSO. Generally speaking, it has the same dynamics and air–sea interactions as the class of simple models (Battisti and Hirst 1988; Suarez and Schopf 1988; Schopf and Suarez 1990; CMZ) that have been used to explain the workings of ENSO. It is quite similar to that of Schopf and Suarez (1990), except that they usually neglect higher ($N > 1$) Rossby waves and so do not find the more complex behavior our model exhibits when several Rossby waves are retained.

The basic oscillation may require only one or two Rossby waves, but our results suggest this oscillation is unstable to perturbations which include higher Rossby waves. Thus, in our results, the higher Rossby waves can change the period of the system and even induce chaos. This occurs although the meridional form we choose for the forcing, being concentrated at the equator, makes the amplitudes of the higher modes relatively small [viz. Fig. (4). $b_5/b_1 = 0.05$, and the factors involving μ and r further reduce the effect of the $N = 5$ mode]. In this regard our model is consistent with previous results indicating that the Rossby wave component in coupled numerical models (Battisti 1989) and the oceanic response to observed winds (Zebiak 1989) is concentrated in the low N, low-latitude modes. So it may be, that despite its relatively small size, the off-equatorial response in nature also influences the period of the coupled system. The inclusion of higher latitudes creates a longer mean period and chaos. Possibly, this mechanism is a role for the off-equatorial signals documented by White et al. (cf. Graham and White 1988 and references therein), which is neither causal nor trivial. This is all the more likely because the real wind system anomalies have larger amplitudes off the equator than our model system.

While the papers cited above all offer fairly similar accounts of the ENSO cycle and why it oscillates, there is no agreement on what sets the characteristic period or what is reponsible for the aperiodicity. In the light of their numerical model results, Schopf and Suarez (1988) and Battisti (1988) suggest that the irregularity of the ENSO cycle is a consequence of natural "noise" such as the intrusion of higher frequency midlatitude effects into the tropics. We do not have a certain explanation for the lack of chaos in their numerical models. Perhaps the higher Rossby waves needed to destabilize the periodic solution are too slow to survive the higher dissipation rates in these models. That possibility is consistent with the results reported here. In any case, the clear implication of the present work is that ENSO could be intrinsically chaotic; no noise is required to explain the observed aperiodicity.

Battisti and Hirst (1989) suggest that the period of the ENSO oscillation is set by a linear mechanism, the balance between dissipation and the inherent instability of the tropical Pacific ocean–atmosphere interactions. The role of nonlinearity is to be dissipationlike and limit the amplitude of unstable modes. Here we are suggesting that the most basic period is quasi-biennial, and that the observed period of approximately 4 years comes about through period doubling and the transition to chaos; the mechanism choosing the preferred period is in essence nonlinear.

It is obvious from the observations that ENSO is aperiodic, but the historical time series is too short to apply methods for identifying dynamical chaos with any certainty. Perhaps the ability of a model to forecast

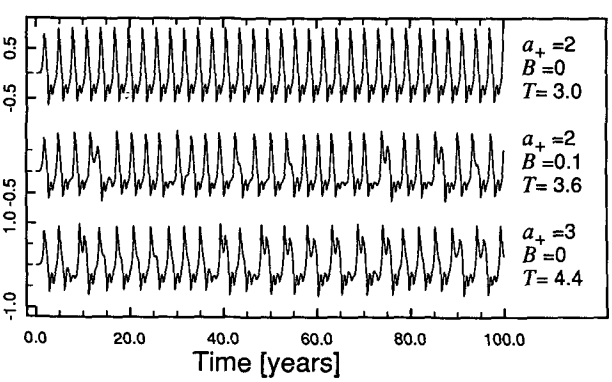

FIG. 7. $h(t)$ for asymmetric forcing. $a_- = 3a_+$, $b_+ = 1.0$, $b_- = 0.5$, $N = 10$, $\kappa = 1.9$. Top: No annual cycle, $a_+ = 2$. Middle: Weak annual cycle, $B = 0.1$; $a_+ = 2$. Bottom: No annual cycle, $a_+ = 3$.

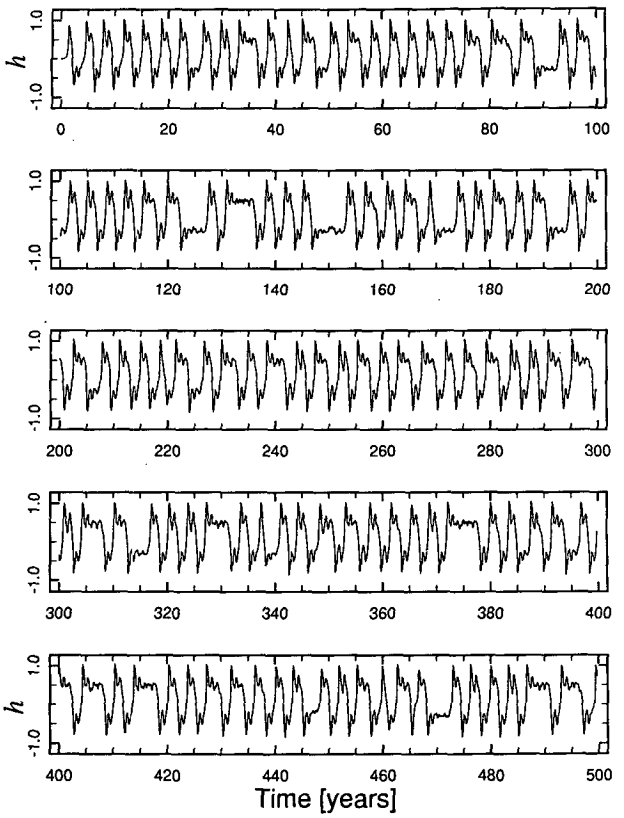

FIG. 8. $h(t)$ for asymmetric forcing and an annual cycle. $\kappa = 2.1$, $a_{\pm} = 5$, $b_{+} = 1$, $b_{-} = 0.6$, $B = 0.2$, $N = 4$.

is evidence in its favor (cf. Barnett et al. 1988), but it is far from decisive.

The model results of Zebiak and Cane (1987) give some support to the period doubling thesis: they show a low amplitude quasi-biennial fluctuation accompanying the dominant quasi-4-year ENSO oscillation. There is also a suggestion of a quasi-biennial component in the tropical Pacific observational record (e.g., Rasmusson et al. 1990; Barnett 1990). Additional work, both observational and theoretical, will be needed to elucidate the quasi-biennial patterns and explore whether the observed quasi-biennial features lend support to the ideas proposed here.

APPENDIX

Deriviation of the Delay Equation

Consider the scaled shallow water equations on the equatorial beta-plane:

$$\begin{aligned} u'_t + yv' + h'_x + ru' &= F', \\ v'_t - yu' + h'_y + rv' &= G', \\ h'_t + u'_x + v'_y + rh' &= H'. \end{aligned} \tag{A1}$$

As usual t stands for time, x and y denote longitudinal and meridional distances, u and v the velocities in these direction and h the equivalent depth. Partial derivatives are written as subscripts. F, G, H are the forcing functions and r is a frictional parameter. If we introduce new variables u, v, h by $u = u' \exp(rt)$, $v = v' \exp(rt)$, $h = h' \exp(rt)$ (A1) becomes formally inviscid:

$$\begin{aligned} u_t + yv + h_x &= F = F'e^{rt}, \\ v_t - yu + h_y v &= G = G'e^{rt}, \\ h_t + u_x + v_y &= H = H'e^{rt}. \end{aligned} \tag{A2}$$

We take the Fourier transform of (A2) with respect to x and obtain

$$\mathbf{u}_t(k, y, t) + \Omega(k, y)\mathbf{u}(k, y, t) = \mathbf{F}(k, y, t) \tag{A3}$$

with

$$\Omega(k, y) = \begin{pmatrix} 0 & -y & ik \\ y & 0 & \partial_y \\ ik & \partial_y & 0 \end{pmatrix}.$$

The free wave solutions of (A2) are of the form

$$\Phi_{n,j}(k, y)e^{i(kx-\omega_{n,j}t)} = \begin{pmatrix} \Phi^1_{n,j} \\ \Phi^2_{n,j} \\ \Phi^3_{n,j} \end{pmatrix}(k, y)e^{i(kx-\omega_{n,j}t)}$$

where the $\Phi_{n,j}$ are the eigenvectors and the $i\omega_{n,j}$ the eigenvalues of $\Omega(k, y)$. These are the well-known gravity, Rossby and Kelvin waves; viz. Cane and Sarachik (1976) from where we adopt our notation. As shown there, these waves form a complete set. We may therefore expand $\mathbf{F}$ and $\mathbf{u}$ in these waves:

$$\mathbf{F}(k, y, t) = \sum_{n,j} f_{n,j}(k, t)\Phi_{n,j}(k, y), \tag{A4}$$

$$\mathbf{u}(k, y, t) = \sum_{n,j} u_{n,j}(k, t)\Phi_{n,j}(k, y), \tag{A5}$$

where the $f_{n,j}(u_{n,j})$ are the projections of $\mathbf{F}(\mathbf{u})$ onto $\Phi_{n,j}$ defined by

$$\begin{aligned} f_{n,j} &= \frac{(\mathbf{F}, \Phi_{n,j})}{(\Phi_{n,j}\Phi_{n,j})} \\ &= \frac{\int_{-\infty}^{\infty} (F^*\Phi^1 + G^*\Phi^2 + H^*\Phi^3)dy}{\int_{-\infty}^{\infty} (\Phi^{1*}\Phi^1 + \Phi^{2*}\Phi^2 + \Phi^{3*}\Phi^3)dy}. \end{aligned} \tag{A6}$$

Inserting (A6) in (A3) yields the following equation for the coefficients

$$\frac{\partial u_{n,j}}{\partial t} + i\omega_{n,j}(k, t)u_{n,j} = f_{n,j}(k, t). \tag{A7}$$

We make the long-wave, low-frequency approximation: we neglect the gravity waves ($j = 1, 2$) and con-

sider the Rossby waves as being nondispersive. Denoting the Kelvin wave by $n = -1$

$$\omega_{-1,1} = \omega_{-1} = k$$

$$\omega_{n,3} = \omega_n = -\frac{k}{2n+1} \quad n = 1, 2, 3, \cdots \quad \text{(A8)}$$

We take the forcing $\mathbf{F}$ to be of the form

$$\mathbf{F}(x, y, t) = A(t)\delta(x - x_0)e^{(-\mu/2)y^2} \cdot \begin{pmatrix} 1 \\ 0 \\ 0 \end{pmatrix}.$$

Cane and Sarachik (1981) give the projections of $\exp(-\mu y^2/2)$ onto the Kelvin and Rossby modes:

$$f_{-1,1} = A(t)\delta(x - x_0)r_{-1} = A(t)\delta(x - x_0)\frac{\pi^{1/4}}{(1+\mu)^{1/2}}$$

$$f_{2n,3}(k, t) = 0 \quad \text{(A9)}$$

$$f_{2n+1,3}(k, t) = A(t)\delta(x - x_0)r_{2n+1} = -f_{-1,1} \times \frac{2\alpha_{2n+1}(1-\mu)^n}{(1+\mu)^{n+1}}\left(\mu + \frac{1}{4n+3}\right) \quad \text{(A10)}$$

with

$$\alpha_{2n+1} = \frac{[(2n+1)!]^{1/2}}{2_n n!}.$$

If we Fourier transform (A7) with respect to time we get, using (A8) and the fact that $\exp(-ikx_0)$ is the Fourier transform of $\delta(x - x_0)$,

$$u_n(k, \omega) = \frac{f_n(k, \omega)}{i(\omega + \omega_n)} = A(\omega)e^{-ikx_0}r_n \Big/ \left[i\left(\omega - \frac{k}{2n+1}\right)\right]$$

and so

$$u_n(x, \omega) = \frac{A(\omega)r_n}{2\pi}\int_{-\infty}^{\infty} e^{ik(x-x_0)} \Big/ \left[i\left(\omega - \frac{k}{2n+1}\right)\right]dk, \quad n = -1, 1, 3, \cdots, \quad \text{(A11)}$$

where we wrote u_n for $u_{n,j}$ and u_{-1} for $u_{-1,1}$. This integral can be evaluated by using the fact that $1/ik$ is the Fourier transform of the Heaviside function $H(x)$. We obtain

$$u_n(x, \omega) = A(\omega)r_n H(x_0 - x)(2n+1)e^{i(2n+1)\omega(x-x_0)}, \quad \text{for} \quad n > 0,$$

$$u_{-1}(x, \omega) = A(\omega)r_{-1}H(x - x_0)e^{i\omega(x-x_0)} \quad \text{(A12)}$$

Summing these contributions we find a solution for the forced shallow water equations

$$\mathbf{u}_{\text{forc}}(x, y, \omega) = \sum_{\substack{n=1 \\ n \text{ odd}}}^{\infty} A(\omega)r_n H(x_0 - x) \times (2n+1)e^{i(2n+1)\omega(x-x_0)}\Phi_n(y) + r_{-1}A(\omega)H(x - x_0)e^{-\omega(x-x_0)}\Phi_{-1}(y).$$

The general solution consists of the forced solution plus the free solution of arbitrary amplitude.

$$\mathbf{u}_{\text{gen}} = \mathbf{u}_{\text{forc}} + \mathbf{u}_{\text{free}} = \sum_{\substack{n=1 \\ n\text{odd}}}^{\infty} (a_n + A(\omega)r_n H(x_0 - x) \times (2n+1)e^{-i(2n+1)\omega x_0})\Phi_n e^{i(2n+1)\omega x} + (a_{-1} + A(\omega)r_{-1}H(x - x_0) \times (2n+1)e^{i\omega x_0})\Phi_{-1}e^{-i\omega x}. \quad \text{(A13)}$$

The a_n and a_{-1} will be determined by the boundary conditions. At the eastern boundary ($x = x_e$) the longitudinal speed has to vanish $u(x_e) = 0$. Now v is small in the low-frequency approximation as concluded in Cane and Sarachik (1976) and we see from the second equation of (A2) that u and h are in geostrophic balance. Now if $u = 0$ as it is at the boundary it follows from $yu + h_y = 0$ that $h(y)$ is constant. Cane and Sarachik [1977, Eq. (23)] gives the following expansion of $\mathbf{u} = (0, 0, h_e)^{\mathrm{T}}$

$$\begin{pmatrix} 0 \\ 0 \\ h_e \end{pmatrix} = h_e\pi^{1/4}\left(\Phi_{-1} + \sum_{\substack{n=1 \\ n \text{ odd}}}^{\infty} 2\alpha_n\Phi_n\right). \quad \text{(A14)}$$

Comparing the coefficients of (A13) at $x = x_e$ and (A14) gives

$$a_n e^{i(2n+1)\omega x_e} = 2\alpha_n\pi^{1/4}h_e(\omega),$$

$$\alpha_{-1}e^{-i\omega x_e} + A(\omega)r_{-1}e^{i\omega(x_0-x_e)} = \pi^{1/4}h_e(\omega). \quad \text{(A15)}$$

The boundary condition at the western end of the basin is not as straightforward as the one on the eastern side. Cane and Sarachik (1977) concluded that for the low-frequency approximation the correct western boundary condition is that the meridional integral of the zonal velocity has to vanish. So if the western boundary is at $x = 0$:

$$\int_{-\infty}^{\infty} u\,(x = 0, y, \omega)\,dy = 0.$$

To compute this we need the zonal integrals of the Kelvin and the Rossby waves. These were given in Cane and Sarachik (1981):

$$\int_{-\infty}^{\infty} \Phi_{-1}^1\,dy = \pi^{1/4}; \quad \int_{-\infty}^{\infty} \Phi_n{}^1\,dy = \frac{\pi^{1/4}\alpha_n}{2n(n+1)}$$

for n odd.

We insert (A15) into (A13) and compute

$$\int udy = 0 = \sum_{\substack{n=1 \\ n \text{ odd}}} 2\alpha_n h_e(\omega) e^{-i(2n+1)\omega x_e}$$

$$+ \sum_{\substack{n=1 \\ n \text{ odd}}} A(\omega) r_n (2n+1) e^{-i(2n+1)\omega x_e} \int \Phi_n^1 dy$$

$$+ (\pi^{1/4} h_e(\omega) e^{i\omega x_e} - A(\omega) r_{-1} e^{i\omega x_e}) \int \Phi_{-1}^1 dy;$$

$$h_e(\omega) = A(\omega) \frac{r_{-1}}{\pi^{1/4}} e^{-i\omega(x_e - x_0)}$$

$$+ \sum_{\substack{n=1 \\ n \text{ odd}}}^{\infty} A(\omega) \frac{r_n (2n+1)\alpha_n}{2n(n+1)\pi^{1/4}} e^{-i(2n+1)\omega x_0 - i\omega x_e}$$

$$+ \sum_{\substack{n=1 \\ n \text{ odd}}}^{\infty} \frac{\alpha_n^2}{n(n+1)} h_e(\omega) e^{-i(2n+2)\omega x_e}. \quad \text{(A16)}$$

Now let $2j - 1 = n$,

$$b_j = \frac{\alpha_{2j-1}^2}{(2j-1)2j},$$

$$a_j(\mu) = \left(\frac{1-\mu}{1+\mu}\right)^{j-1} \frac{[(4j-1)\mu + 1]}{1+\mu}, \quad \text{(A17)}$$

and use (A9) and (A10) in (A16) to obtain

$$h_e(\omega) = \frac{A(\omega)}{(1+\mu)^{1/2}} e^{-i\omega(x_e - x_0)}$$

$$- \frac{1}{(1+\mu)^{1/2}} \sum_{j=1}^{\infty} A(\omega) b_j a_j(\mu) e^{i(4j-1)\omega x_0 - i\omega x_e}$$

$$+ \sum_{j=1}^{\infty} b_j h_e(\omega) e^{-i\omega 4 j x_e}. \quad \text{(A18)}$$

Transforming (A18) into the time domain yields (3) of the main text.

REFERENCES

Barnett, T., 1990: The interaction of multiple time scales in the tropical climate system. *J. Climate,* **3,** 269–285.

——, N. Graham, M. A. Cane, S. E. Zebiak, S. Dolan, J. J. O'Brien and D. Legler, 1988: On the prediction of the El Niño of 1986–1987. *Science,* **241,** 192–196.

Battisti, D. S., 1988: Dynamics and thermodynamics of a warming event in a coupled tropical atmosphere–ocean model. *J. Atmos. Sci.,* **45,** 2889–2919.

——, 1989: On the role of off-equitorial oceanic Rossby waves during ENSO. *J. Phys. Oceanogr.,* **19,** 551–559.

——, and A. C. Hirst, 1989: Interannual variability in the tropical atmosphere–ocean system: Influence of the basic state and ocean geometry. *J. Atmos. Sci.,* **46,** 1687–1712.

Bjerknes, J., 1969: Atmospheric teleconnections from the equatorial Pacific. *Mon. Wea. Rev.,* **97,** 163–72.

Cane, M. A., 1986: El Niño. *Ann. Rev. Earth Planet. Sci.,* **14,** 43–70.

——, and E. S. Sarachik, 1976: Forced baroclinic ocean motions I: The linear equatorial unbounded case. *J. Mar. Res.,* **34,** 629–664.

——, and ——, 1977: Forced baroclinic ocean motions II: the linear equatorial bounded case. *J. Mar. Res.,* **35,** 395–432.

——, and ——, 1981: The response of a linear baroclinic equatorial ocean to periodic forcing. *J. Mar. Res.,* **39,** 651–93.

——, S. E. Zebiak and S. C. Dolan, 1986: Experimental forecasts of El Niño. *Nature,* **321,** 827–832.

——, M. Münnich and S. E. Zebiak, 1990: A study of self-excited oscillations of the tropical ocean atmosphere system. Part I: Linear analysis. *J. Atmos. Sci.,* **47,** 1562–1577.

Collet, P., and J. P. Eckmann, 1982: *Iterated Maps of the Interval as an Dynamical Systems.* Birhäuser, 248 pp.

Eckmann, J. P., 1981: Roads to turbulence in dissipative dynamical systems. *Rev. Mod. Phys.,* **53,** 643–653.

Graham, N. E., and W. B. White, 1988: The El Niño–Southern Oscillation as a natural oscillation of the tropical Pacific ocean–atmosphere system: evidence from observations and models. *Science,* **240,** 1293–1302.

Rasmusson, E. M., X. Wang and C. F. Ropelewski, 1990: The biennial component of ENSO variability. *J. Mar. Syst.,* **1,** 70–96.

Schopf, P. S., and M. J. Suarez, 1988: Vacillations in a coupled ocean–atmosphere model. *J. Atmos. Sci.,* **45,** 549–566.

——, and ——, 1990: Ocean wave dynamics and the timescale of ENSO. *J. Phys. Oceanogr.,* **20,** 629–645.

Suarez, M. J., and P. S. Schopf, 1988: A delayed action oscillator for ENSO. *J. Atmos. Sci.,* **45,** 3283–3287.

Vallis, G. K., 1986: El Niño: A chaotic dynamical system? *Science,* **232,** 243–245.

——, 1988: Conceptual models of El Niño and the Southern Oscillation. *J. Geophys. Res.,* **11,** 979–991.

Wyrtki, K., 1975: El Niño—the dynamic response of the equatorial Pacific Ocean to atmospheric forcing. *J. Phys. Oceanogr.,* **5,** 572–584.

Zebiak, S., 1989: Oceanic heat content variability and El Niño cycles. *J. Phys. Oceanogr.,* **19,** 475–486.

——, and M. A. Cane, 1987: A model El Niño–Southern Oscillation. *Mon. Wea. Rev.,* **115,** 2262–2278.